OPTICAL CHARACTERIZATION OF MATERIALS IN THE MID-WAVE INFRARED

Thesis

Submitted to

The School of Engineering of the

UNIVERSITY OF DAYTON

In Partial Fulfillment of the Requirements for

The Degree of

Master of Science in Electro-Optics

By

Jordan David Page

UNIVERSITY OF DAYTON

Dayton, Ohio

August, 2024

OPTICAL CHARACTERIZATION OF MATERIALS IN THE MID-WAVE INFRARED

Name: Page, Jordan David

APPROVED BY:

Paul McManamon, Ph.D.
Advisory Committee Chairman
Professor, Electro-Optics and
Photonics

Rita Peterson, Ph.D.
Committee Member
Professor, Electro-Optics and
Photonics

Andrew Sarangan, Ph.D.
Committee Member
Professor and Chair, Electro-Optics
and Photonics

ABSTRACT

OPTICAL CHARACTERIZATION OF MATERIALS IN THE MID-WAVE INFRARED

Name: Page, Jordan David
University of Dayton

Advisor: Dr. Paul McManamon

Material characterization begins with finding the refractive index of the respective materials. The goal of this thesis is to develop a method to find the refractive index utilizing a high-power tunable mid-wave infrared (MWIR) laser.

The general techniques used to determine the refractive index using this laser follow the principles of the Fresnel equations of reflection and transmission coefficients. By collecting the Reflectance and Transmittance we can then determine the refractive index following the equations.

Amid starting to use the laser there was a sudden and gradual drop in the laser power. From there the refractive index measurements turned into tests on the laser itself to find the root of the power drop. With a detour of working directly on the laser to provide the correct wavelength and adequate power began the direction of this thesis to find a reasonable method of finding the refractive index with this laser in its current state. While completing the multitude of refractive index tests, we explore the internal components of the laser and how it functions.

Dedicated to my family for their continuous support.

ACKNOWLEDGMENTS

I would like to acknowledge my advisor Dr. Paul McManamon for general guidance throughout this journey of completing the refractive index measurements and tests on the laser in efforts to fix the problems.

Another acknowledgement goes to Cullen Bradley who assisted and guided for the material preparation process and assistance to use the MWIR laser for the first time.

Lastly acknowledgement goes to Dr. Rita Peterson for her continuous support and outstanding knowledge of the laser system. Without here assistance and teaching me of the laser system I would not have the expanded knowledge I have today.

TABLE OF CONTENTS

LIST OF FIGURES

LIST OF TABLES

LIST OF VARIABLES

Below is a list of variables used

n	Refractive Index
κ	Optical Extinction coefficient
λ	Wavelength
$\mathcal{R}$	Reflectance
$\mathcal{T}$	Transmittance
I	Measured Power/Intensity
d	thickness

LIST OF ACRONYMS

Below is a list of acronyms

$BaTiO_3$	Barium Titanate
CdTe	Cadmium Telluride
FTIR	Fourier-Transform Infrared
$KNbO_3$	Potassium Niobate
$LiNbO_3$	Lithium Niobate
MWIR	Mid-wave Infrared
OPGaAs	Orientation-Patterned Gallium Arsenide
OPO	Optical Parametric Oscillator
PMN-PT	Lead Magnesium Niobate - Lead Tantalate

CHAPTER I

INTRODUCTION

Optical characterization begins with finding the refractive index. The goal of this work is centered around determining the refractive index of different material in the mid-wave infrared (MWIR) region. We explore the MWIR spectrum as different applications look to progress into this region, for example thermal imaging, free-space optical communications, and within the defense sector for missile detection or military surveillance. To assist with the beginning steps of exploring these applications the materials we look at needed to be characterized in the MWIR region. From here the first property to explore in any circumstance is the index of refraction. The refractive index of any material is widely used and need for any modeling or analysis. In some applications it is best to have the exact or an estimate to this value rather than interpolating the results from previous literature.

The refractive index of a optical medium is a dimensionless value defined as the ratio of the speed of light in vacuum to the speed of propagation in the medium. The index of refraction, n, varies with wavelength thus causing dispersion. Common developments of refractive index characterization focuses on the creation of a dispersion formula to determine the refractive index of a material at any inputted wavelength. These formulas change based on the gathered data values as they are simply a fit to the refractive index results. Furthermore the refractive index is not always real there can be an imaginary component, κ. This imaginary component accounts for the loss by absorption within the material. While scattering is considered loss and is present in some cases it does not count for the loss considered in the imaginary component of the refractive index. The materials in this work have some properties which showcase birefringence. Birefringence is based on the physical properties of the material and due to these differences, the speed of propagation is

a function of direction[2]. Based on the physical properties and orientation of the crystal it will determine the refractive index that would be solved for in the later tests.

This project stems from previous work through material exploration for electro-optic (EO) modulators in the near infrared spectrum. The stages from that project was designed to coincide with this thesis by transitioning the wavelength region from the near infrared to the mid-wave infrared. The aspect of that work was to find the refractive index and the EO coefficient of the materials in question. The materials we explore for these tests are: Lithium Niobate ($LiNbO_3$), Potassium Niobate ($KNbO_3$), Barium Titanate ($BaTiO_3$), Cadmium Telluride (CdTe), and Lead Magnesium Niobate Lead Tantalate (PMN-PT). Additional materials that were explored in the near-infrared but not pursued in this work are: Barium Borate (BBO), KBN, and KTN. Currently in the world $LiNbO_3$ is the most dominant material when it comes to EO modulators, while the other materials we explore can produce higher speeds with a lower power based on the EO coefficient of the material. Based on the same idea of exploring alternate materials for a variety of applications, however the goal was to expand into the MWIR spectrum. Applications like EO modulators normally operate at the telecom wavelength of 1550 nm, it has the potential to be used in the MWIR. Another application of exploring these materials is within the regime of imaging for non-destructive testing, biomedical, and help with thermal imaging. No matter the application that the material is to be used for, the refractive index within the MWIR spectrum needs to be characterized and studied.

There are plenty of methods used to find the refractive index of material used today. Two of the most common methods of determining the index of refraction is ellipsometry and minimum deviation. Ellipsometry focuses on taking a ratio of the polarization states of light and its interaction on a thin film on substrate. The minimum deviation method utilizes

a prism cut and oriented in a certain angle to obtain precise measurement results. We look into and compare this method to one used for the results displayed in this study. Based on the goal of using the specific laser and the type of material samples collected we explore a method derived from the principles of Fresnel equations for reflection and transmission. While this method will not provide the most accurate result, it provides a general estimate of the refractive index for modeling purposes. In terms of the results obtained through these methods they allow accurate precision for the modeling purposes.

The first method was confirmed at a wavelength within the near-infrared (1550 nm), but the goal was to explore these materials utilizing a high-power tunable MWIR laser. Upon transitioning to using the MWIR laser in the lab, many complications were presented with the laser. With the complications of the laser, the methods needed adapting for the specific wavelength region and to accommodate the power produced by the laser. This thesis report speaks on the materials that were chosen to explore, the complications of the laser, and showcase the results of the index of refraction through each different configuration of the testing setup.

CHAPTER II

BACKGROUND

2.1 Fresnel Equations

One of the most fundamental topics in optics is the Fresnel equations. These equations—derived by Augustin-Jean Fresnel in 1823—describe the interaction between light and an optical interface. Prior to deriving the Fresnel equations we have to consider two different conditions where the electric field vector is either perpendicular or parallel to the plane of incidence, otherwise known as S-polarization and P-polarization respectively [2]. After the understanding of the polarization states we can begin the derivation of these equations based on the boundary conditions at the interface. As visual representation figure 2.1 [3] shows the field vectors of the light waves assuming S-polarization.

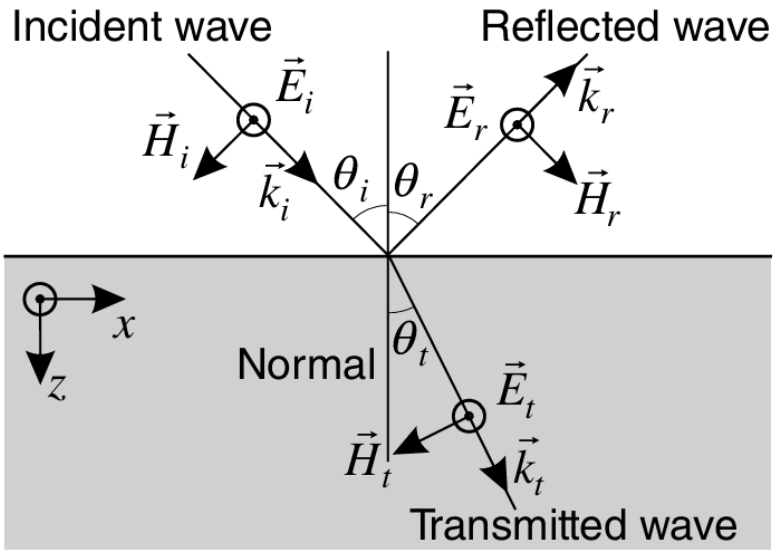

Figure 2.1: Field vectors of the light waves assuming S-Polarization.

Starting with Maxwells equations relating the Electric field to the Magnetic field we have,

$$H_{i,r} = \frac{n_1}{c} E_{i,r} \quad \text{and} \quad H_t = \frac{n_2}{c} E_t \tag{2.1}$$

The boundary conditions of an S-polarized wave is as followed,

$$E_i + E_r = E_t \tag{2.2}$$

$$-H_i \cos\theta_i + H_r \cos\theta_i = -H_t \cos\theta_t \tag{2.3}$$

With the known boundary conditions, we start with an expanded version of (2.2) in terms of the magnetic field,

$$\frac{1}{n_1}(H_i + H_r) = \frac{1}{n_2} H_t \tag{2.4}$$

Finally substituting (2.4) into (2.3), we derive the Fresnel equations assuming S-polarization,

$$r_s = \frac{E_r}{E_i} = \frac{n_1 \cos\theta_i - n_2 \cos\theta_t}{n_1 \cos\theta_i + n_2 \cos\theta_t} \tag{2.5}$$

$$t_s = \frac{E_t}{E_i} = \frac{2n_1 \cos\theta_i}{n_1 \cos\theta_i + n_2 \cos\theta_t} \tag{2.6}$$

Following the same derivation path with the following boundary conditions,

$$E_i \cos\theta_i + E_r \cos\theta_i = E_t \cos\theta_t \tag{2.7}$$

$$H_i - H_r = H_t \tag{2.8}$$

we derive the following equations assuming P-polarization.

$$r_p = \frac{E_r}{E_i} = \frac{n_1 \cos\theta_t - n_2 \cos\theta_i}{n_1 \cos\theta_t + n_2 \cos\theta_i} \tag{2.9}$$

$$t_p = \frac{E_t}{E_i} = \frac{2n_1 \cos\theta_i}{n_1 \cos\theta_t + n_2 \cos\theta_i} \tag{2.10}$$

2.2 Refractive Index Measurement Techniques

Early on when new materials would be characterized to find the refractive index the most common method was minimum deviation. However as technology advanced different techniques became developed and easier to use for example Ellipsometry and Fourier Transform Infrared (FTIR) spectroscopy. While this study utilizes a suboptimal way to determine the refractive index, its best to look at some alternative methods. The reasoning behind this decision is based on the access to materials and equipment.

2.2.1 Minimum Deviation

The first alternative method we will look at is minimum deviation. The type of material needed for this technique is in the shape of a prism. Ideally when looking though at the side surface of the prism it should be a equilateral triangle. Figure 2.2 shows the rays of the light traversing through the material in this case.

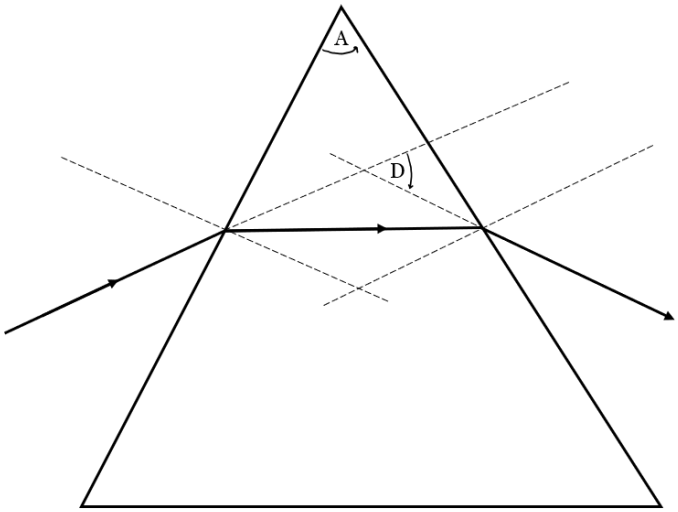

Figure 2.2: Minimum Deviation prism diagram.

The relationship for the refractive index to the angle of minimum deviation is shown by (2.11)[4],

$$n = \frac{\sin\frac{A+D}{2}}{\sin\frac{A}{2}} \tag{2.11}$$

where A is the apex angle of the prism and D is the angle of minimum deviation. How these angles are defined is shown in 2.2. The measurements taken in the lab is the Apex angle and the incident angle into the prism and the exiting angle as well to determine the deviation angle. The one condition for the measurements is the ray within the material needs to be parallel to the base. The big condition to using this method is based on the size and surface quality needed for these measurements. Due to the access to such prism we were unable to use this method.

2.2.2 Ellipsometry

The next alternative method is Ellipsometry. Ellipsometry measures changes in light polarization to determine the material properties[5]. The experimental setup is shown in Figure 2.3 [5]. The laser source is initially not polarized then goes through the a linear polarizer before interaction with the material. After the interaction with the material it produces an elliptically polarized light which is then analyzed and transferred into two values.

The two values measured are an amplitude component Ψ and the phase difference Δ. In other words these two quantities are placed into (2.12) which is the complex reflectance ratio ρ. The complex reflectance ratio is similar to the Fresnel equations (2.9) and (2.5).

$$\rho = \frac{r_p}{r_s} = \tan\Psi e^{i\Delta} \tag{2.12}$$

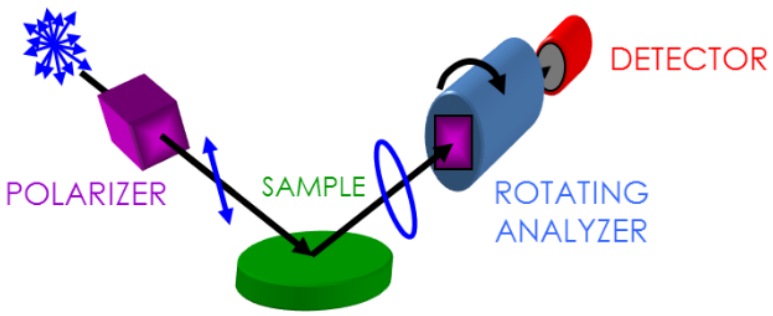

Figure 2.3: Schematic of Ellipsometry.

To determine the refractive index in this system follows a general model developed. Within the model is taken general assumptions of the optical constants and the estimated/known thickness of the material. For this method most commercial ellipsometers come with a software that assists with this analysis.

2.2.3 Fourier Transform Infrared Spectroscopy

The last common method used is FTIR. This method uses the general principle of a Michelson interferometer where two beams are being compared to each other through interference. The beam path in the system has two interactions with the material sample, either be absorbed or be passed through via transmission. The results presented from this method is a absorption and transmission spectrum where it can provide data for several types of material properties [6]. The internal design on most FTIR systems is shown in Figure 2.4[7].

The main advantages to using FTIR spectroscopy revolves around the speed of the measurement and the sensitivity it provides. Along with the analysis of the materials set in place for this measurement technique, the computer would complete the Fourier Transform

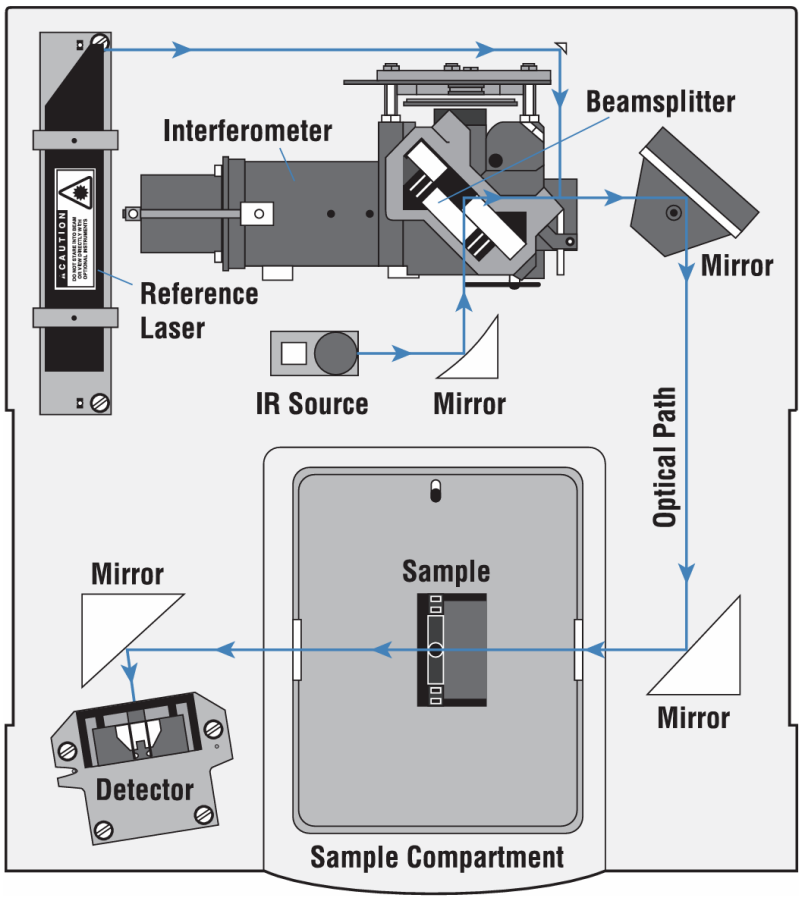

Figure 2.4: Schematic of FTIR spectroscopy design.

and present the percent transmission spectrum to be used for analysis purposes. Another advantage of utilizing FTIR is the capability to explore other material states like liquids and gases. Each material has its own unique spectrum and utilizing this method takes advantage of this principle and can provide information on a material if it is unknown[6].

Using the Fresnel equations is not the only way to find the refractive index of the crystals. While there are advantages to using an ellipsometry method or FTIR spectroscopy to determine the refractive index with the desired wavelength region, the goal was to use the laser discussed later. Ellipsometry is a great technique when you have a thin film on

substrate, however the cost for using this method varies based on the desired wavelength you want to explore. Continuing forward is a look at the materials set up to explore using the Fresnel equations and how they are structured for the tests to find the refractive index.

CHAPTER III

MATERIALS

Out of the materials mentioned before above only $LiNbO_3$ and $KNbO_3$ have been explored in this region, the others need to be further characterized. Based on previous work of using these as alternative materials for EO modulators most we decided upon in that application among determining the EO coefficients. First $LiNbO_3$ was decided simply as a control material to validate each method as it has already been characterized in this wavelength region. Meanwhile, $KNbO_3$ has been characterized for the refractive index it was intially explored for it EO coefficient measurements throughout the infrared region. Additionally BTO and PMN-PT were decided upon based on past measurements of EO coefficients, however PMN-PT needs more characterization overall. Finally CdTe was chosen as it can be utilized in wavelength regions were $LiNbO_3$ is not applicable. Each of these materials needed to be prepared in a certain facet to allow for the measurements to take place.

3.1 Sample Preparation

To allow for the transmission measurements, the sample needs to be polished on both sides. While some of the materials were obtained with one or both sides polished, others needed to be cut and polished. For example, the PMN-PT was grown in the lab and needed to be cut into the appropriate thickness and surface area for the beam to interact. The cutting method consists of using a SYJ-160 low-speed diamond saw manufactured by MTI Corporation. Prior to cutting the material is waxed onto a sacrificial piece of Teflon and the placed on the diamond saw. The diamond saw blade used is around 0.3 mm thick and

runs at a velocity of 120 rpm. With the material eventually cut into the appropriate shape, the next step is to grind/polish the surface to create the optically clear material.

The polishing technique used the UNIPOL 810 polishing machine manufactured by MTI Corporation. To polish the materials, they were first waxed onto a metal disk in preparation for the polishing techniques. To use the polishing machine, first we run water to a small stream on top of the diamond lapping plate. With the diamond lapped sheet covered in water we proceed with the polishing as the metal disk with material is carefully placed on the plate. The polishing machine runs at slow speeds (60-90 rpm) until the metal disk is freely rotating. At this point, the material is smooth enough at the designated diamond lapping mesh size. This process starts at a mesh size around twelve microns and repeats until the mesh size is less than a micron. It is important to not rush this process as materials may break during this process if the speed of the polishing is too high. Also to note about the material polishing is it will take less time at the higher mesh size whereas the other is true of more time the smaller the mesh size. Each material was prepared in a certain facet and size as shown in Table 3.1. In the table are the orientation of each crystal from how they are to be used in testing. The orientation of the $LiNbO_3$, $BaTiO_3$, and PMN-PT allow for the measurement of the ordinary refractive index, while the $KNbO_3$ will provide the *c*-axis for the result. Since CdTe is a semiconductor it will only have the one refractive index to measure.

3.2 Lithium Niobate

The main material worked on throughout this thesis was $LiNbO_3$ due to it being widely characterized. The specific material samples obtained for this work was gathered by MTI Corporation with both sides polished. $LiNbO_3$ in the aspect of optics and use in optical

Table 3.1: List of Materials and their respective size for measurements.

Material	Size (mm)	Orientation
$LiNbO_3$	10x10x1	X-cut
$KNbO_3$	10x10x1	Z-cut
$BaTiO_3$	10x10x0.5	(0 0 1)
CdTe	3x5x1	(1 1 0)
PMN-PT	10x10x0.5	(1 0 0)

frequency-conversion devices. As mentioned this material has been characterized before by Zelmon *et al.* [8]. In contrast to this work, the study done by Zelmon uses the minimum-deviation method to determine the refractive index. The minimum-deviation method utilizes the material as a bulk prism cut and oriented in a certain way to view the dispersion. The prism was cut on the x-axis, which provides data for the ordinary refractive index. The apex angle for this method was optically measured as 44.941°. Since $LiNbO_3$ is a birefringent material it consists of two refractive indices relative to the optical axis. One is considered the ordinary, n_o, and the other is the extraordinary, n_e. The measured refractive indices is shown in the figure 3.1.

Continued from the study they were able to develop the dispersion (Sellmeier) formula to determine the refractive index by inputting the desired wavelength. The formula for both the ordinary and extraordinary are presented in the following equations (3.1) and (3.2).

$$n_o^2 = 1 + \frac{2.6734\lambda^2}{\lambda^2 - 0.01764} + \frac{1.2290\lambda^2}{\lambda^2 - 0.05914} + \frac{12.614\lambda^2}{\lambda^2 - 474.60} \tag{3.1}$$

$$n_e^2 = 1 + \frac{2.9804\lambda^2}{\lambda^2 - 0.02047} + \frac{0.5981\lambda^2}{\lambda^2 - 0.0666} + \frac{8.9543\lambda^2}{\lambda^2 - 416.08} \tag{3.2}$$

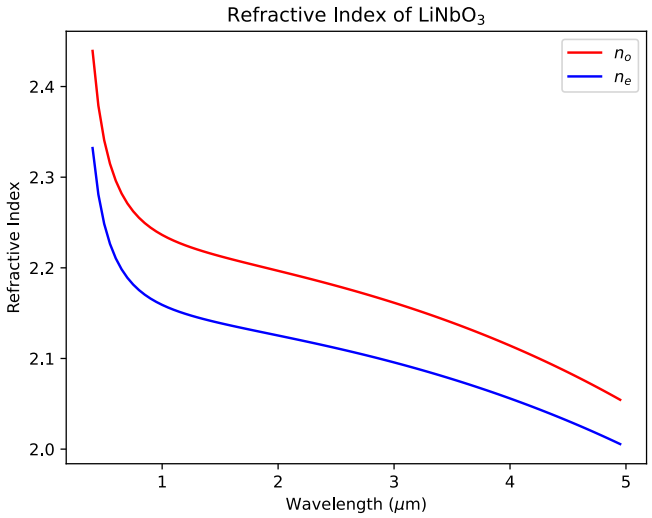

Figure 3.1: Measured Refractive Index results of $LiNbO_3$.

Based on the material cut the refractive index that would be calculated would be the ordinary refractive index. Utilizing (3.1) and looking at 3.1 we can find the the expected result for example assuming $\lambda = 4.2\mu$m the refractive index will be $n = 2.10$.

3.3 Potassium Niobate

The second material set to explore is $KNbO_3$, this material was donated by the AFRL for the purpose of these measurements. This material was already polished on both sides of the sample and was ready for the experiments. The main applications of $KNbO_3$ focuses on its large nonlinear coefficients. The initial aspect of the exploring this material is based on a higher EO coefficient and determining the capability in an EO modulator. However due to $KNbO_3$ having large nonlinear coefficients most applications focus on its nonlinear properties in second-harmonic generation (SHG) and sum-frequency generation (SFG). In the article written by Umemura *et al.* [9], they explore the aspect of phase-matching

within the MWIR. $KNbO_3$ is a biaxial material, therefore it consists of three different refractive indices. To solve for these refractive indices Umemura *et al.* have based some of their work previously on work by Zysset *et al.*[10]. Zysset *et al.* initially developed the Sellmeier equations used to determine the refractive indices. Which are used to determine the expected refractive indices of the experiments. The method used by Zysset *et al.* was the same as Zelmon *et al.* which was the minimum-deviation method. Although Zysset developed the initial Sellmeier equations the following equations (3.3)-(3.5) were developed by Umemura *et al.*. This decision was done based on the wavelength region covered when creating the equations and also the fact of it being more completed recently [9].

$$n_x^2 = 4.4222 + \frac{0.09972}{\lambda^2 - 0.05496} - 0.01976\lambda^2 \tag{3.3}$$

$$n_y^2 = 4.8353 + \frac{0.12808}{\lambda^2 - 0.05674} 0.02528\lambda^2 + 1.8590 \times 10^{-6}\lambda^4 1.0689 \times 10^{6}\lambda^6 \tag{3.4}$$

$$n_z^2 = 4.9856 + \frac{0.15266}{\lambda^2 - 0.06331} 0.02831\lambda^2 + 2.0754 \times 10^{-6}\lambda^4 1.2131 \times 10^{6}\lambda^6 \tag{3.5}$$

From the above equations the following plot 3.2 was created to show each of the refractive indices in a figure for reference over the wide spectrum.

3.4 Barium Titanate

Next material to explore is $BaTiO_3$, this material used for sampling was obtained via MTI Corporation with one side polished. To allow for the transmission measurements we had to polish the other side before the experiments. The reasoning behind using this material is its extremely high EO coefficient and it is becoming more prevalent material in many optical applications. Similar to $LiNbO_3$, this material is uniaxial so it has the ordinary and extraordinary refractive indices, although the only published results of the refractive index is only within the visible spectrum. Based on the work by Wemple *et al.*[1],

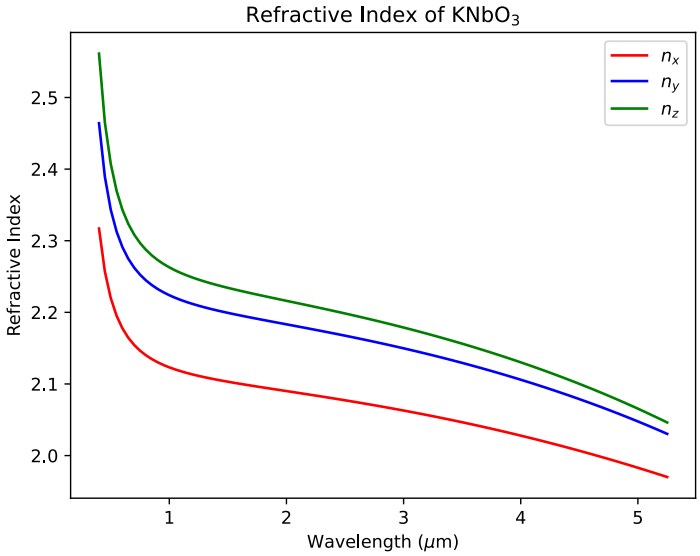

Figure 3.2: Refractive Indices of $KNbO_3$.

the refractive index plots for $BaTiO_3$ within the visible spectrum is shown 3.3. While most optical devices are using either the near infrared or the MWIR regions this material is not characterized for the measured refractive index in those spectral regions. So we chose to progress with this material for measurements.

Continuing from the study completed by Wemple *et al.*, (3.6) and (3.7) were developed for the refractive index results. The problem with this equation revolves around the amount of data points collected and the range. The coefficients within the equation can change significantly if more data points were collected on a larger range of wavelengths.

$$n_o^2 = 1 + \frac{4.187\lambda^2}{\lambda^2 - 0.223^2} \tag{3.6}$$

$$n_e^2 = 1 + \frac{4.064\lambda^2}{\lambda^2 - 0.211^2} \tag{3.7}$$

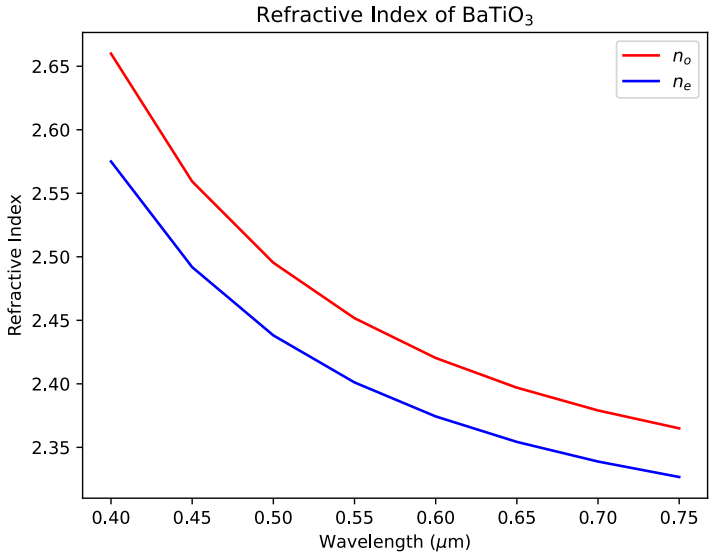

Figure 3.3: Refractive Indices of $BaTiO_3$ [1]

3.5 Cadmium Telluride

The next material chosen to explore is CdTe, this material is different to the others as it is more of a semiconductor material. The sample gathered of CdTe needed to be cut and polished in order for the measurements to be completed. Its most common application is in the form of solar cells, however the goal in this project was to explore its aspect in an EO modulator. Although this material does not seem plausible in the near infrared wavelength it would be best suited for ultraviolet wavelengths. The main issue though is large loss and attenuation at those wavelengths. The refractive index characterization for this material is published from the visible to near infrared regions. This published work was completed by Marple [11], with the main method done as minimum-deviation.

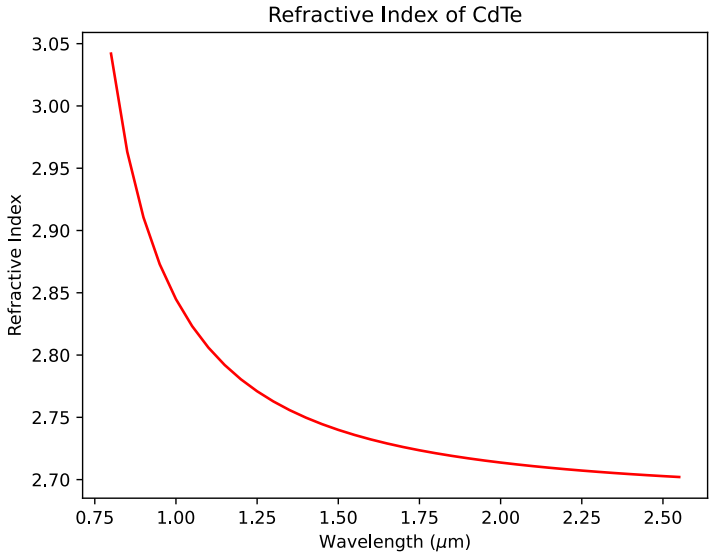

Figure 3.4: Refractive Index of CdTe.

Figure 3.4 showcases the published results for the refractive index. With (3.8) as the dispersion formula for finding the expected index at other wavelengths.

$$n^2 = 5.68 + \frac{1.53\lambda^2}{\lambda^2 - 0.366} \tag{3.8}$$

3.6 Lead Magnesium Niobate - Lead Tantalate

The last material planned to explore is PMN-PT, in comparison to the other materials there is little to no information regarding this material. Based on work completed by Xiao *et al.* they focused on finding the EO coefficient of this ceramic material [12]. From that study the Quadratic EO coefficient was found to be $S_{33} = -2.24 \times 10^{-16} \frac{m^2}{V^2}$. Overall this material has little information regarding the refractive index which brings forth the reasoning to continuing to explore this material in both visible and infrared spectrum. The PMN-PT

material was locally grown and needed to be cut into the desired shape and polished on both sides before using in the experiments.

Each material was collected and prepared (if needed) before the measurements were taken. The material preparation consisted of cutting and polishing for optically transparent materials through equipment manufactured by MTI Corporation. The surface area on the faces of the thin bulk crystals had one dependence to be larger than the diameter of the beam. Although some materials had a valid dispersion formula the goal to verify the refractive index was is place. For the other materials that have little to no information the goal was set forth to determine the refractive index and if possible verify the expected values.

CHAPTER IV

LASER

The laser used throughout the experiments is a high-power tunable MWIR laser. This laser was designed and manufactured by a team at BAE Systems [13] for research purposes at the University of Dayton. The overall design of the laser functions consists of internal and external systems to allow for proper operation. The external system of the laser is shown in 4.1. Prior to the internal components and operation, the external system needs to be powered on. The external equipment stack is used to control the interior components and the power of the laser overall. There is a total of four different electronics within the equipment stack, from top to bottom in 4.1 you have the laser control box, IPG thulium doped fiber laser, dry air generator, and chiller.

Firstly, the laser control box developed by BAE Systems which controls all aspects of the laser and contains the turnkey to operate the laser emission. As shown on the box are a couple of LEDs that will alert the user when the laser is ready and the control state of the humidity within the laser. Within this box is what controls the emission from the fiber laser and via a laptop helps distinguish the angle and temperature of the OPO cavity to allow for proper operation and wavelength emission. For this specific laser, the pump is a thulium doped fiber laser developed by IPG Photonics (50 W, 1.908μm wavelength). The dry air generator manufactured by Thorlabs, and the chiller manufactured by KO-concepts.

The internal aspects of this laser consists of three different stages: fiber laser, Q-switched Holmium-doped Yttrium Aluminum Garnet (Ho:YAG) oscillator, and a mid-wave optical parametric oscillator (OPO) cavity. Under the basic principles of a laser there must be a pump source which in this case is the thulium doped fiber laser. A total of 37 W of 1.908 μm is used to pump the Q-switched Ho:YAG oscillator. The oscillator converts the 1.908

Figure 4.1: External electronics stack for laser operation.

μm into another lasing wavelength of 2.09 μm. The Ho:YAG oscillator emits up to 11 W of 2.09 μm at repetition rate of 10 kHz from there a total of 5 W of the 2.09 μm light is used to pump the mid-wave OPO. The other 5 W of 2.09 μm light would be used to pump another OPO system for Long-wave infrared(LWIR) light. While this upgrade feature is not in this iteration of the laser it currently goes into a beam dump eliminate the excess light inside the laser head. These individual stages are displayed in 4.2.

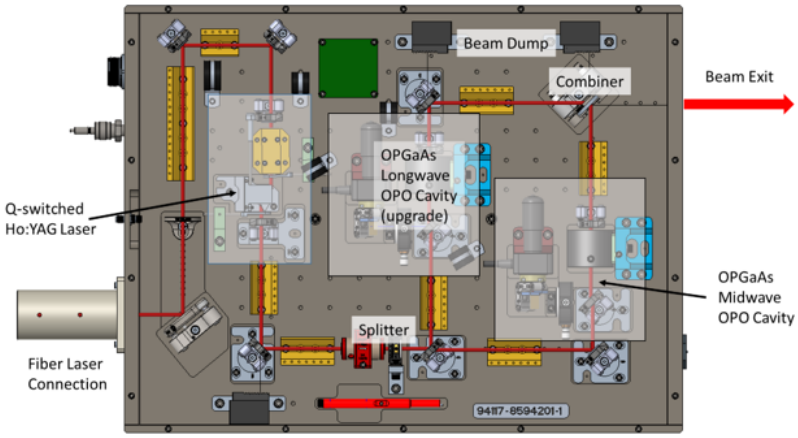

Figure 4.2: Schematic of the Laser Head stages for Mid-wave IR emission.

An OPO cavity functions by a nonlinear frequency conversion to convert the pump frequency into two lower frequencies. Within the OPO cavity is a nonlinear crystal, the crystal used in this system is orientation-patterned gallium arsenide (OPGaAs). The OPO is a common method to produce the wavelengths within the MWIR. From the general principles of nonlinear conversion, the interaction of the pump source and the nonlinear crystal will produce the signal and idler wavelengths. To allow for any conversion at all, the OPO must meet phase-matching conditions. The tunable feature comes at changing the phase-matching conditions[14], some ways to do this is by changing the refractive index of the material, changing the angle of the crystal (material dependent), and in the case of this laser is to change the temperature of the nonlinear crystal. For example, this laser uses a temperature unit to control the temperature of the crystal to assist with the phase-matching conditions. Shown in the plot 4.3 we can explore the data provided by BAE Systems[13] of the measured wavelength vs the temperature of the crystal. The vertical line represents the maximum temperature of the temperature control unit, which controls the tunable range of the laser to be from 3576-5037 nm. With the signal band 3576-4180 nm and the idler

band 4180-5037 nm. The primary wavelength emitted from the laser is determined by the grating position and the temperature of the crystal as both these variables work together to produce the phase-matching conditions.

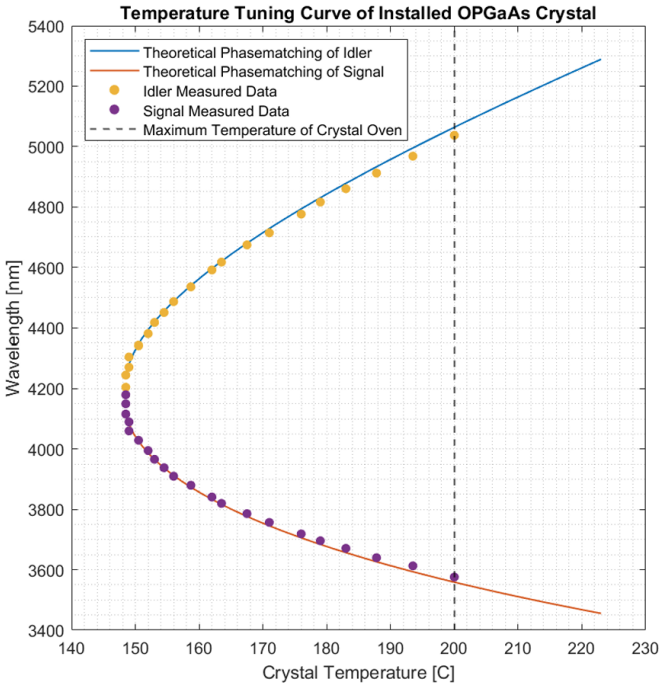

Figure 4.3: Wavelength vs. OPGaAs crystal temperature experimental data.

4.1 Operation of the Mid-wave Infrared Laser

With an understanding of the external and internal components of the laser we are able to proceed to using the laser. The first step to powering on the laser is to turn on all the external components. Starting with the laser control box and then turning the key of the IPG fiber laser. Once the key for the fiber laser is switched, the dry air generator and chiller need to be powered on by their local switches. The dry air generator should have a flow rate of 3. Afterwards we can start the emission of the fiber laser. Although the

emission light is on for the fiber laser, the emission will not happen until the turnkey on the laser control box is turn on FIRE. At this point, the humidity within the laser head needs to be around three percent which will take about 30-60 minutes depending on the surroundings and the consistency of using the laser. Once the 'LASER READY' LED is green, the external electronics for laser operation are complete.

To control the internal components of the OPO we need to utilize the laptop above the equipment stack. Provided by BAE Systems is a text file which consists of three columns of calibration data for the desired wavelength, temperature of crystal, and grating angle. Along with the file is two different software, one to change the temperature of the temperature control unit holding the nonlinear crystal and the other to change the grating angle within the OPO cavity. The grating angle adjusts what wavelengths are allowed to resonate within the cavity, while the temperature controls the phase-matching to produce the desired wavelengths from the OPO in the MWIR. Before firing the laser the main condition to meet is the stability of the temperature. Once the temperature is stable within 0.03 degrees Celsius we can turn the key and begin observing the beam out the laser head.

For the first time using the laser, we ran some preliminary tests to understand the laser properties. Since the laser has essentially three different wavelengths exiting the laser head, a low-pass is placed at an angle right at the exit to block the pump wavelength. From there we only see the signal and idler based on the desired wavelength. At this point we determined the polarization of the beam is linear in the vertical position relative to the optical table. Furthermore, the next test was to observe the beam power over the course of time. This test was completed to know how much time it would take for the laser to fully stabilize, so we can begin the refractive index tests. From figure 4.4 it is shown as an

approximate wait of 10 minutes until power of signal and idler combined stabilizes upon startup.

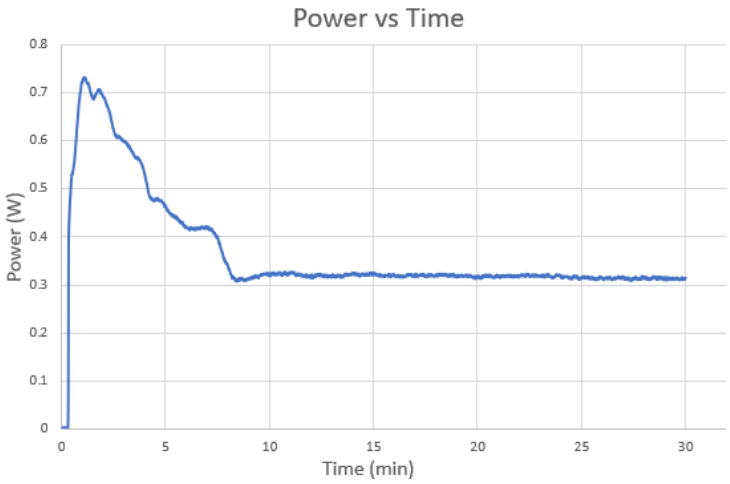

Figure 4.4: Power vs Time to view stability of the laser upon startup.

Secondly, the next test was a variation of power and time but changing the wavelength. In the test we go from the initial turn on wavelength of 3800 nm to 3750 nm. This test shows how much time we must wait after changing the wavelength before the next data set can be taken. Based on the design we can change the wavelength and grating while the emission is still active. Figure 4.5 shows the time it takes for the power of signal and idler to stabilize upon changing the wavelength.he wavelength. Something to note about the sudden drop and increase of the laser power is based on the temperature and the phase-matching within the OPO cavity to produce the desired changed wavelength.

Both of these test show the power of the signal and idler of the laser with blocking of the pump wavelength, and they were both consistent with the data provided by the company [13] while they were developing the laser. However while these tests help understand the

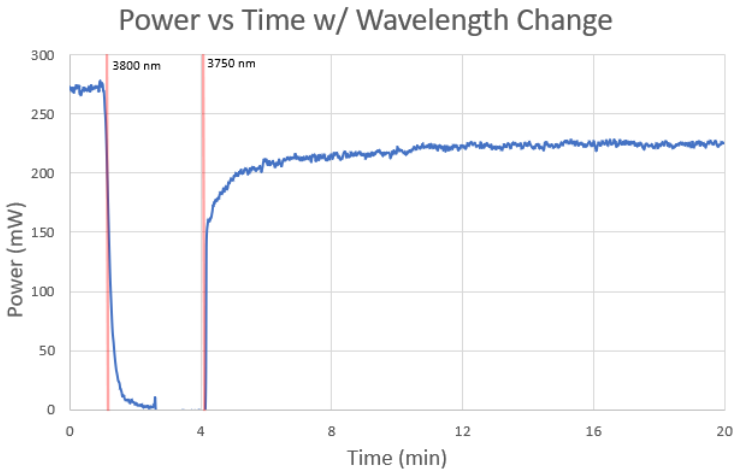

Figure 4.5: Power vs Time of laser based on a change in wavelength.

laser, there were complications upon using the laser regularly. For example, there was a sudden then gradual drop in the laser power over time and by viewing the laser directly on a detector sheet we can visibly see two beams. In the case of using an OPO and also having the pump, the beams should overlap and not be separate.

4.2 Complications with the Laser

With consistent use of the laser over the course of a week there was a sudden drop in the power. What once produced 300 mW of power was now down to around 100 mW. The questions of why this was happening was brought up in conversation with the developers of the laser at BAE Systems. They brought forth a couple of questions regarding the beam shape, the calibration, and the alignment of the system overall. A simple test performed is shown in Table 4.1. The wavelength used for the test is 3800 nm and the normal temperature of the crystal should be 165.85°C. From the table we can see a small displacement of the temperature, but it is not a large difference to warrant any change in the calibration data.

Table 4.1: Power of the laser based on Temperature change.

Temperature ($C°$)	Power (mW)
160.0	35.87
161.0	36.55
162.0	36.23
163.0	37.61
164.0	47.33
165.0	60.32
166.0	122.07
167.0	129.71
168.0	102.14
169.0	63.38
170.0	41.01

Based on data gathered from a knife's edge experiment the beam shape was then calculated by taking the derivative. Figure 4.6 shows the raw data and the calculated beam shape from the data. In this experiment there appears to have a change in the beam shape as it is not a clean Gaussian curve as expected. Further discussion of the beam shape occurred with the people at BAE Systems, and the following expectation was to use a Mid-IR camera to view the beam profile.

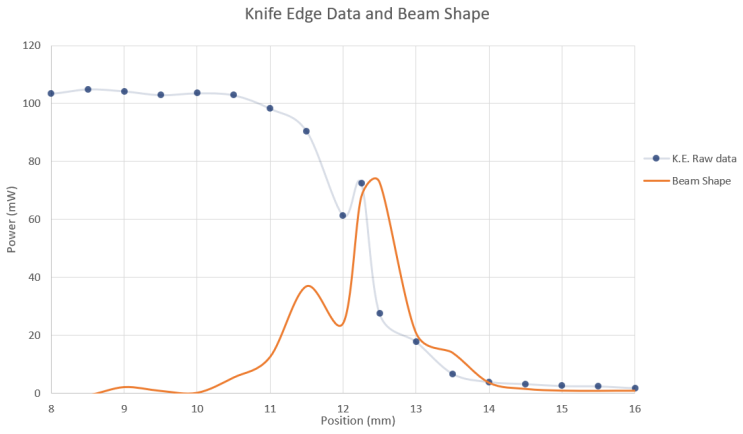

Figure 4.6: Knife Edge experiment data with the analyzed beam shape.

As shown above the laser was functioning properly for the first couple of days using the laser. After the couple of days the laser suddenly began to drop in power. As shown in 4.4 the power was around 300 mW. The questions and work then progressed to trying to diagnose the problem and speak to the company. Through various tests brought forth by the company there was an inconclusive understanding of the problem and a method to fix. The work then progressed and the next power vs time test was done and it is shown in 4.7.

Throughout the course of time we repeated the power vs time measurements to document the change in the power produced by the laser. Figure 4.7 shows the next power vs time test completed. The stability of the laser remained the same throughout with 10 minutes before stabilizing, however as shown the power now stabilized around 80 mW of the signal and idler with the pump source blocked. The problem remained the same with the power gradually dropping, however the goal remained the same to determine the refractive index of the different materials.

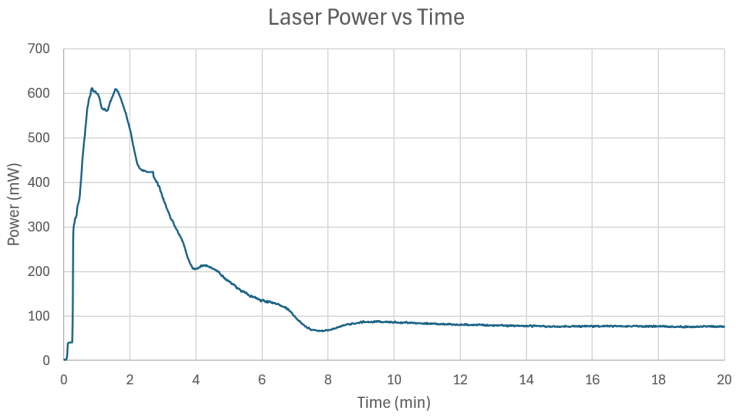

Figure 4.7: Power vs Time of the laser upon startup to observe the power drop.

One final test to assist with the laser power was to explore what the power is at each wavelength used for testing. This plot 4.8 shows how much the variation is over time and among each of the wavelengths. To note, in this test is no low-pass filter in place, so this power is a combination of residual pump, signal, and idler. This was done just to showcase the power of the laser in its general state through the majority of the tunable region.

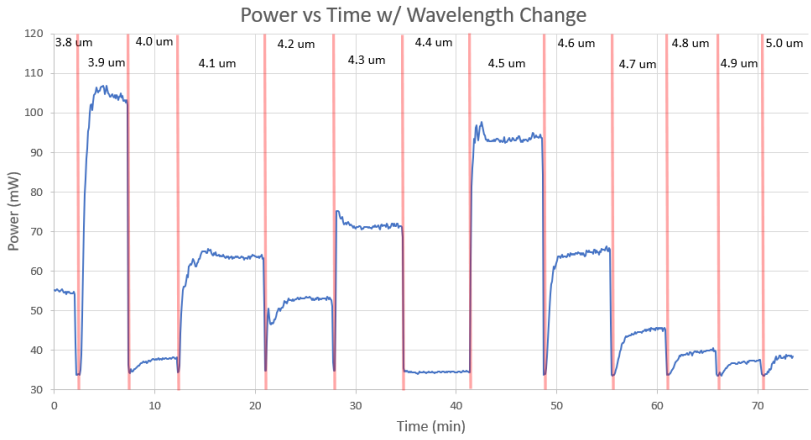

Figure 4.8: Power vs Time with continuous wavelength change upon stabilization.

Upon completion of the refractive index methods the power of the laser with a low-pass filter in place to block both pump and signal wavelengths, the idler provided an average of 10 mW. While no filter was situated within the system the power averaged around 40 mW. With the testing methods completed and knowing the laser needed to be fixed, the decision led towards opening the laser and determining where the power drop was occurring. Figure 4.9 shows what the power was in the corresponding location. To accommodate the detectors (max of 5W) we lowered the power output of the fiber laser. The first power measurement was set to determine the power after the Ho:YAG oscillator which was around 4.7 W. Following that through the optics and the interaction of a beam splitter the power was then

halved to provide 2.1 W of power into the OPO cavity (boxed in Yellow). Within the OPO cavity the power was still high and was around 1.8 W. Finally the power after the OPO cavity the power was around 35 mW. Upon leaving the laser head the power was around 14 mW which is what would be provided for all the refractive index tests. The drop for 35 mW to 14 mW is because there is a filter in place to help reduce the power from the pump.

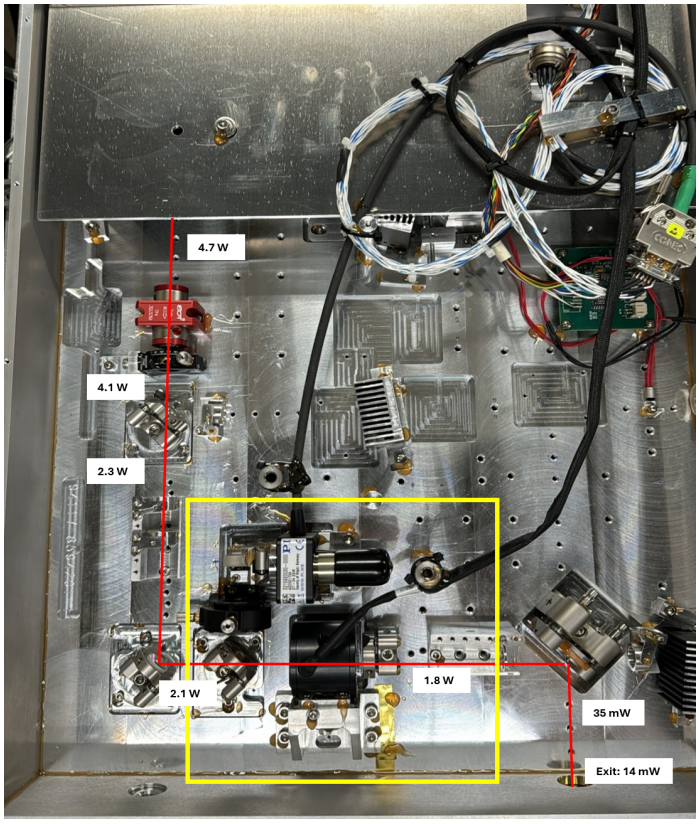

Figure 4.9: Laser Head with the measured Power at each stage.

Each of these power drops are consistent when compared to the initial power drops assuming the fiber laser is operating at the normal 37 W. Noticing the power drop after the OPO begged to question what is the problem. Some thoughts were initially the calibration

or damaged optics, looking carefully at each of the optics proved the point of a damaged optic which was the OPGaAs crystal shown in Figure 4.10. The small dot circled in red is the damage point on the crystal which is thought as the main contribution to the laser power drop.

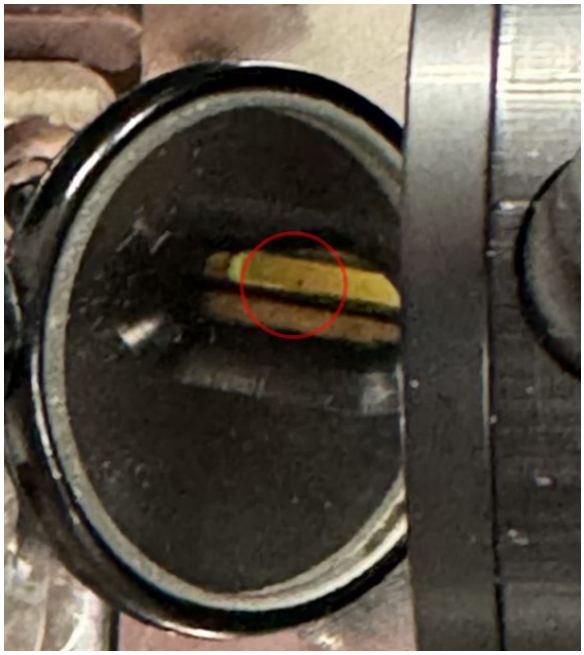

Figure 4.10: Damage on the surface of the crystal inside the temperature control unit.

The laser was initial up to specifications from the company, but suddenly dropped in power. Although the laser was continually dropping in power based on every time using the laser, the refractive index measurements were to proceed as planned. Once the measurement data points were taken was the point to open the laser and try and see the problem which was found as the damage on the crystal. As precaution to the next user of the laser it should be fixed and each of the basic tests should be done regularly to continue to observe and monitor the damage of the crystal so it can be replaced.

CHAPTER V

REFRACTIVE INDEX METHODS

Following the understanding of the laser, we can begin working on the different methods of determining the refractive index. Although the more common methods to determine the refractive index of materials are Ellipsometry, FTIR spectroscopy, and method of minimum deviation. The goal to finding the refractive index by using the Fresnel equations was influenced by two factors: 1) using the MWIR laser in the lab, 2) the condition of the materials obtained. Each of the following methods are based on the general equations of reflection and transmission coefficients with some basic derivations based on what is expected and assumed.

5.1 Transmission at Normal Incidence

The first method explored considers the power measured via transmission at normal incidence, shown in figure 5.1. This setup is easy as we measure the power at two positions, before and after the material. This was the first method explored due to simplicity of the set up configuration and the general assumptions that we were able to make based on the material.

Initially this method was completed at 1550 nm with the $LiNbO_3$ and we can take the value of the refractive index to be real considering the loss at this wavelength is negligible. Taking these assumptions into account we obtain the following equations to determine the refractive index.

$$R = \left| \frac{1 - n_2}{1 + n_2} \right|^2 \tag{5.1}$$

Rewriting (5.1) to solve for n_2,

$$n_2 = \frac{1 - \sqrt{R}}{1 + \sqrt{R}} \tag{5.2}$$

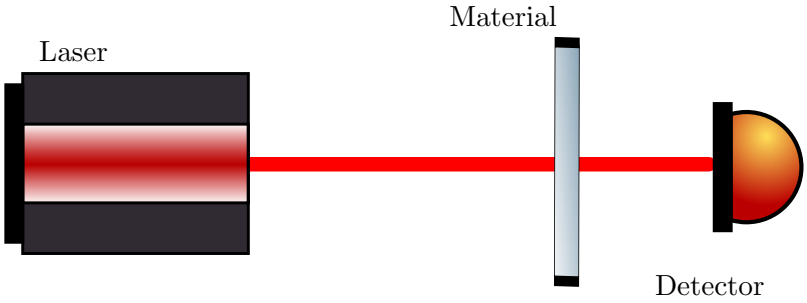

Figure 5.1: Transmission at normal incidence diagram

Under the minimal loss assumption we use (5.3). Along with this assumption is the data gathered in the lab which is designated as (5.4), where I_0 is the power of laser incident on the material and I_T is the power of the laser after the transmission through the material.

$$R + T = 1 \tag{5.3}$$

$$T = \frac{I_T}{I_0} \tag{5.4}$$

Taking the above equations and the applying substitutions we can utilize (5.5) to find the refractive index in this method.

$$n_2 = \frac{1 - \sqrt{1 - \sqrt{\frac{I_T}{I_0}}}}{1 + \sqrt{1 - \sqrt{\frac{I_T}{I_0}}}} \tag{5.5}$$

As mentioned above this method was done at a lower wavelength and general conditions and assumptions were made. Moving forward into the MWIR laser the method was tested again, but the assumptions appeared to be invalid. By no longer being able to use these assumptions the method to find the refractive index needed to be changed. The next method explored was to measure the reflection and transmission of the laser and its interaction with the material sample.

5.2 Reflection and Transmission Measurement

As spoken above utilizing the transmission at normal incidence for $LiNbO_3$ in the MWIR region is not possible under the previous assumptions. Therefore, the experiment using the MWIR laser needed changing to use both reflection and transmission measurements to determine the refractive index. Through different iterations of the setup the final setup is shown in figure 5.2. Directly at the output of the laser is a low-pass (LP) filter at the 4130 nm wavelength (Spectrogon Longwave-Pass 4130 Filter). According to the data sheet from the filter there is over 90 percent transmission of the wavelengths above the designed wavelength (4130 nm).

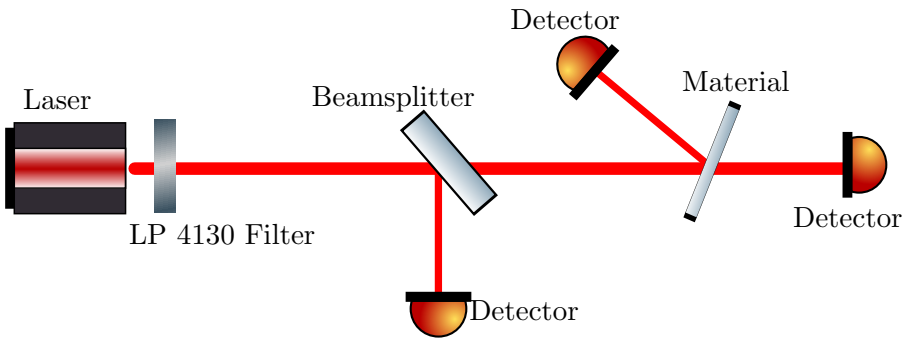

Figure 5.2: Simultaneous measurement of reflection and transmission diagram.

In the setup is a beam splitter (Thorlabs BSW 510) that was incorporated, so the three measured data points can be collected at the same time. According to the specification sheet provided by Thorlabs, the beam splitter is supposed to be 50:50 however this was not the case and in either case the power divided by the beam splitter needs to be calibrated at each wavelength of measurement as it can vary as shown in Table 5.1. The ratio displayed

is the reflected over the transmitted (R/T) to help find the incident power on the material by collecting the reflected power off the beam splitter.

Table 5.1: Calibrated Beam Splitter Ratio to determine the incident power on the material.

Wavelength (nm)	Calibrated Beam Splitter Ratio
4200	0.317
4400	0.40
4600	0.25
4800	0.357
5000	0.305

Finally, the data collected was measured at three points: 1) Power reflected by the beam splitter (Incident), 2) Power transmitted through the beam splitter but reflected by the material (Reflection), and 3) Power transmitted through the beam splitter but transmitted through the material (Transmission). From the data collected different data analysis methods were explored, double surface reflection, transmission at an angle of incidence, and single surface reflection. Each method of analysis explored uses the value θ_2, which is the angle transmitted in the material. Through Snell's Law (5.6) we are able to derive 5.9

$$n_1 \sin\theta_1 = n_2 \sin\theta_2 \tag{5.6}$$

Rewriting Snell's law,

$$\sin\theta_2 = \frac{n_1}{n_2} \sin\theta_1 \tag{5.7}$$

Using the basic trigonometry principle of Pythagorean Theorem

$$\cos^2\theta_2 + \sin^2\theta_2 = 1 \tag{5.8}$$

Finally substituting (5.7) into (5.8) and solving for $\cos\theta_2$

$$\cos\theta_2 = \sqrt{1 - \frac{n_1^2}{n_2^2}\sin^2\theta_1} \tag{5.9}$$

Another thing to note about these methods and equations relates to what is being solved as the refractive index. Each equation is written with n_2, which takes an assumption of the real part of the refractive index. While doing the analysis of the measurements the refractive index was assumed this way along with some still in progress work of using the refractive index to be complex as shown in (5.10). Where n_2 is the real part, and κ is the imaginary component also know as the optical extinction coefficient. The analysis with the imaginary component follows a general substitution of the refractive index of the equations with the complex refractive index.

$$n^* = n_2 + i\kappa \tag{5.10}$$

5.2.1 Double Surface Reflection

From the data collected by the previous setup 5.2 we first look at the aspect of double surface reflection. Since the materials being explored are polished on both sides, we need to account for the second surface reflection within the material. The derivation of this analysis is provided by Born and Wolf[15]. The assumptions taken for this derivation is minimal loss (5.3), and the imaginary component in this equation relates to a change in phase among the reflection through the material.

First we start with the general equation of Fresnel equations with the interaction of a single surface,

$$r_{12} = \frac{n_1\cos\theta_1 - n_2\cos\theta_2}{n_1\cos\theta_1 + n_2\cos\theta_2} \tag{5.11}$$

Then incorporating the reflection from the second surface is,

$$r_{23} = \frac{n_2 \cos\theta_2 - n_3 \cos\theta_3}{n_2 \cos\theta_2 + n_3 \cos\theta_3} \tag{5.12}$$

Lastly the overall expression of the reflection becomes,

$$r = \frac{r_{12} + r_{23} e^{2i\beta}}{1 + r_{12} r_{23} e^{2i\beta}} \tag{5.13}$$

where β consists of interaction within the material,

$$\beta = \frac{2\pi}{\lambda} n_2 d \cos\theta_2 \tag{5.14}$$

The Reflectance which is measured from the experiment can then be written as (5.15)

$$\mathcal{R} = |r|^2 = \frac{r_{12}^2 + r_{23}^2 + 2 r_{12} r_{23} \cos 2\beta}{1 + r_{12}^2 r_{23}^2 + 2 r_{12} r_{23} \cos 2\beta} \tag{5.15}$$

5.2.2 Transmission with Angle of Incidence

Continuing with the data collected by 5.2, we now utilized the transmission data collected. This analysis method follows the same principles of the double surface reflection of assuming minimal loss, therefore the sum of the Transmittance and Reflectance should be one. Following the same set of equations derived from [15] we gather the following equation sets.

$$t_{12} = \frac{2 n_1 \cos\theta_1}{n_1 \cos\theta_1 + n_2 \cos\theta_2} \tag{5.16}$$

$$t_{23} = \frac{2 n_2 \cos\theta_2}{n_2 \cos\theta_2 + n_3 \cos\theta_3} \tag{5.17}$$

From here the overall transmission coefficient becomes,

$$t = \frac{t_{12} t_{23} e^{2i\beta}}{1 + r_{12} r_{23} e^{2i\beta}} \tag{5.18}$$

Finally the Transmittance measured in the experiments would be (5.19),

$$\mathcal{T} = |t|^2 = \frac{t_{12}^2 t_{23}^2}{1 + r_{12}^2 r_{23}^2 + 2r_{12}r_{23}\cos 2\beta} \tag{5.19}$$

As a final check to the assumption of minimal loss of absorption we can substitute (5.15) and (5.19) into (5.3). By a straightforward calculation we can obtain this result.

5.2.3 Single Surface Reflection

The next method explored with the data set from the previous setup, but also via a new setup as shown in figure 5.3. Since the materials in the previous methods had both surfaces polished we needed to have a rough back surface for this new assumption. In order to obtain the rough surface a piece of scotch tape was applied to limit the back surface reflection and allowable transmission.

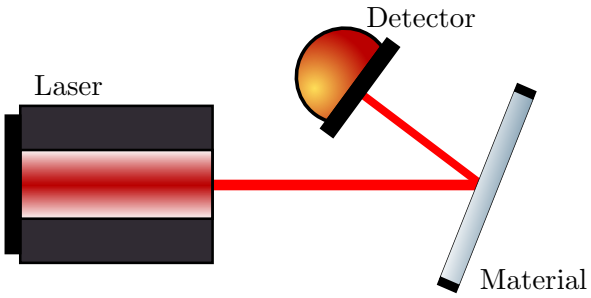

Figure 5.3: Single Surface Reflection diagram

With the assumption of no back surface reflection, the equation is based on the initial interaction of the laser with the front surface.For this method we use (5.20) to determine the refractive index. Same as the other equations the polarization is a big factor in the

equations, as it determines the combination of refractive index and angle.

$$R_{\perp} = (\frac{n_1 \cos\theta_1 - n_2 \cos\theta_2}{n_1 \cos\theta_1 + n_2 \cos\theta_2})^2 \tag{5.20}$$

5.3 Single Wavelength Transmission Measurement

The final method explored is based on a paper written by Bastin *et al.*[16]. Here we take two distinct transmission measurements at a single wavelength. Bastin *et al.* follow the general principle of an integrating sphere to distinguish the loss of absorption and scattering in solids. They explored three different cases based on material assumptions, only scatter (μ) light, only absorb (ω) light, and both scatter and absorb (Σ) light (5.21).

$$\Sigma = \mu + \omega \tag{5.21}$$

Based on the assumptions made they were able to determine (5.22) to incorporate the loss and Reflectance to the Transmittance by including the thickness, d, of the material.

$$\frac{I_T}{I_0} = \frac{(1-R)^2 e^{-\Sigma d}}{1 - R^2 e^{-2\Sigma d}} \tag{5.22}$$

In order to utilize this equation for refractive index purposes we explore the aspect of system of equations with two equations and two unknowns. The two unknowns in this circumstance are the refractive index of the material, n, and the loss term, Σ. Assuming the interaction of the laser and the material at normal incidence we obtain the first equation (5.23).

$$\mathcal{T} = \frac{I_T}{I_0} = \frac{(1 - (\frac{n-1}{n+1})^2)^2 e^{-\Sigma d}}{1 - (\frac{n-1}{n+1})^4 e^{-2\Sigma d}} \tag{5.23}$$

For the second equation we take into account an angle of incidence on the material which results in (5.24),

$$\mathcal{T} = \frac{I_T}{I_0} = \frac{(1 - (\frac{n\cos\theta_2 - \cos\theta_1}{n\cos\theta_2 + \cos\theta_1})^2)^2 e^{\frac{-\Sigma d}{\cos\theta_2}}}{1 - (\frac{n\cos\theta_2 - \cos\theta_1}{n\cos\theta_2 + \cos\theta_1})^4 e^{\frac{-2\Sigma d}{\cos\theta_2}}} \tag{5.24}$$

To accommodate the interaction and change of optical path length through the material, we had to apply the angle change in the exponential term. With both equations derived we are now able to explore this method in detail and compare to the other methods.

All the above methods incorporate the Fresnel Equations in some way to find the refractive index. The testing procedure consisted of multiple data sets to compare the data from day to day and each data set was used in their respective analysis. Along with the analysis to find the refractive index we take two assumptions, only solving for the real component of the refractive index and the assumption of a complex refractive index (5.10) to include the extinction coefficient by the loss of the material. Overall each method should be straightforward in determining the refractive index based on theory, however as shown in the next section the results do not appear to match.

CHAPTER VI

RESULTS

While the goal is to explore the other materials, the primary material explored for each measurement method was $LiNbO_3$. The reasoning behind only trying to use $LiNbO_3$ is based on the functional aspect of the laser. With the power fluctuations and the power consistently lowering after each use, it was best to try and find which method is best to use for this laser. The analysis of each method was completed in a simple Python code shown in Appendix A.

6.1 Transmission at Normal Incidence Results

The first method explored was transmission at normal incidence. The first test of this method was done at 1550 wavelength to confirm the method and compare with widely known values. Figure 6.1 shows the different data points collected for the refractive index and the horizontal line is at the expected value for the $LiNbO_3$, $n = 2.21$.

From the values collected of the refractive index using (5.5) for each data point and then taken the average over all the data points. The average over the data is calculated as $n_{avg} = 2.22$, which is comparable to the expected and proves this method is valid in this wavelength region under the assumptions used for the method. With the proof of concept complete for the transmission at normal incidence complete we then moved the setup to use the MWIR laser. Following the same procedure and using the same assumptions we are able to obtain the following results in figure 6.2 over the course of the tunable range at step size of 100 nm. between each data point. Through the spectrum we utilize (3.1) to calculate the expected results for comparison. Included in the figure is a general trend of the refractive index through the spectrum. Based on the significant difference between

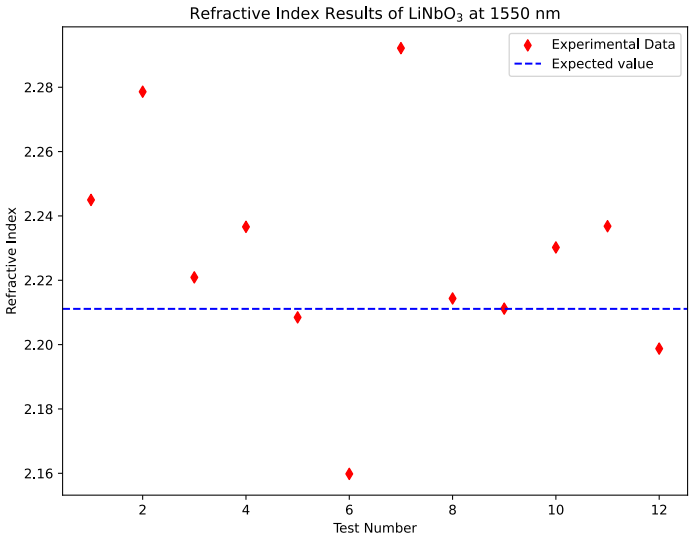

Figure 6.1: Refractive Index Results of $LiNbO_3$ at 1550 nm.

the expected and experimental refractive index, the general assumptions made using this method is no longer valid when using this wavelength region for $LiNbO_3$.

6.2 Reflection and Transmission Measurement Results

The understanding of not being able to apply the previous assumptions led to the a change in the method. The change in method looked at measuring the reflection and transmission at the same time to obtain the refractive index and compare the result from the equations. While this method was designed to overcome any power fluctuations of the laser, the results did not align with the expected. We utilized (5.15) and (5.19) to solve for the refractive index. The parameters used for these tests include, a 20 degree angle of incidence ($\theta_1 = 20°$, a total of 30 seconds of power was averaged on the detector, and the polarization of the laser is configured for vertical polarization. Figure 6.3 shows the data collected and analyzed through the double surface reflection method. From the results there

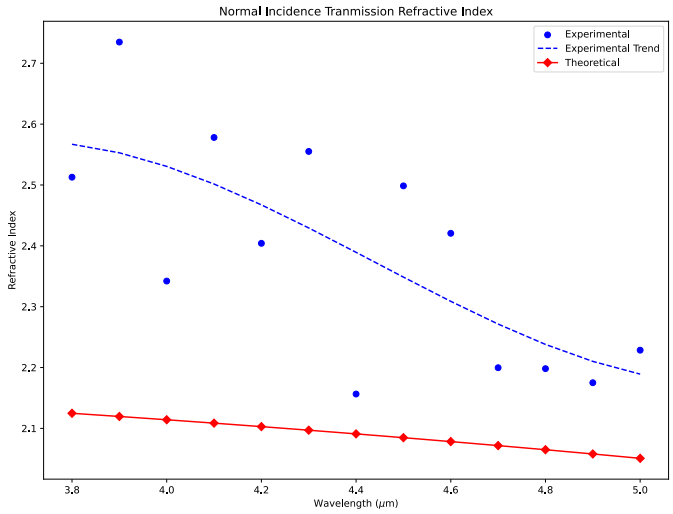

Figure 6.2: Refractive Index Results of $LiNbO_3$ in the MWIR using Transmission at Normal Incidence.

is some promise from the trend of the points, however it is well above the expected results. Some problems in the data collection led to the interaction of material as reflection and transmission values would be greater than one which shows no loss from the material.

From the same parameters and gathered at the same time, we analyze the transmission data with (5.19). Figure 6.4 displays the expected and experimental data from the two data sets. The main problem with these results are based around the calculated refractive index is measured around 1.15, which is around half the expected result. Similar to the reflection results it seems promising based on trend, but the value is not reasonable. In the reasonable case the measured refractive index of the material using the two analysis methods for reflection and transmission the value should be equal to each other or very close in value.

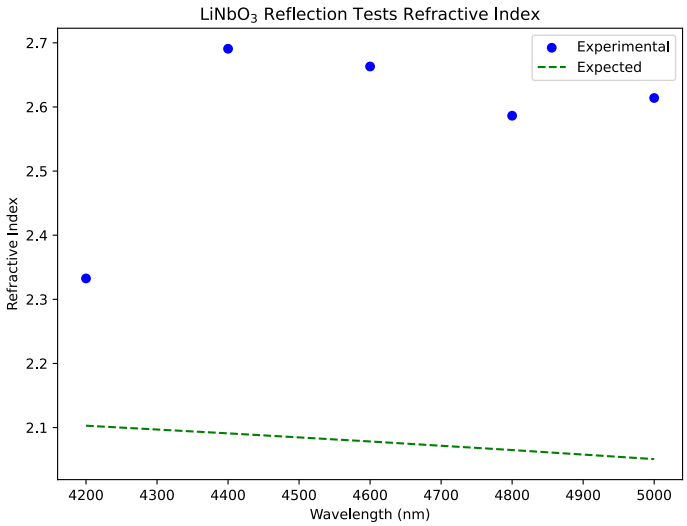

Figure 6.3: Refractive index results from the two reflected datasets.

Even though all the data was collected at the same time, questions are brought up on the calculated refractive index. The first question revolves around the power produced from the laser and the raw data collected as such low power levels. Another question regarding the measurement is controlling what wavelength is being produced and interacting with the material sample. As refractive index is a function of wavelength, we need to control what the wavelength is being emitted from the laser. If more than one wavelength is interacting with the material this can be a main problem in the results. These questions are currently being explored as future work with the laser progresses and as the laser continues to be used, these questions should be addressed.

Overall as the main results of the do not match the expected results we then explored the laser at one wavelength and tried to compare each method and find one that would be best suited to find the refractive index. The material used for the comparison was $LiNbO_3$, and the wavelength chosen was 4.2 microns. At this wavelength the refractive index should

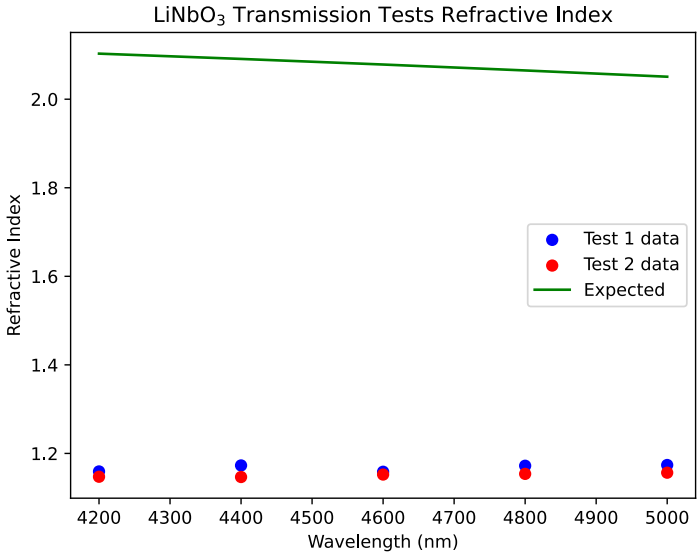

Figure 6.4: Refractive index results for two transmission datasets.

be around 2.1. Using this wavelength allows only viewing the idler beam in the system and provided adequate power for the measurements. Table 6.1 shows the comparison between each method and the calculated refractive index.

Table 6.1: Comparison of each method at 4.2 micron wavelength.

Method	Calculated Refractive Index
Single Reflection	2.5505
Double Reflection	2.3325
Normal Transmission	2.4041
Angled Transmission	1.159

The final test method to explore was the utilizing the system of equations based on transmission data at different angles. The results from this method were much more complex

to find with finding two unknowns and the displayed results were as follows: $n = 1.34, \mu = 3.39$. Solving the equation 5.22 with the known values, we obtain $T = 0.78$ at $\theta = 0°$. These values of transmission do not match with the transmission data collected, which was $T = 0.682$. From the results not lining up to the expected results the loss has a big factor. The loss in some cases is not only through absorption, but rather through scattering which aligns not with the method or analysis but the material surface state. In summary most issues with the data collection utilizing this laser is based on the power obtained and being produced from the laser. Under the completion of the analysis the most promising would be utilizing the double surface reflection equation for analysis and technique to find the refractive index. Overall the complications with the laser prolonged the accuracy of the measurements for analysis.

CHAPTER VII

CONCLUSION

With the results completed there are still questions to be answered to understand with method explored would produce the most accurate and reasonable estimation of the refractive index. While the methods explored are sub optimal in comparison to ellipsometry, FTIR spectroscopy, and minimum deviation, they were best used for the two goals of the thesis which were using the MWIR laser and explore the refractive index of materials in the tunable region of the laser. Overall the method of minimum deviation will provide the most accurate result of refractive index, the only problem limiting use of this method was the material samples obtained were thin bulk crystals. Where the material sample could then be implemented into an ellipsometer or a FTIR spectrometer, the limiting factor on ellipsometer was access to an ellipsometer that allows the MWIR spectrum. Similarly the FTIR might have been another option, but it would not use the laser. However using the FTIR spectrometer would be an ideal way to check the results from these different tests.

Besides questioning the method techniques we can begin to look at the laser and its condition. Based on the laser there is at least two questions, can we increase the power for these measurements and what is the definitive wavelength interacting with the material surface. At time of writing, current efforts are in place to fix the laser power. Since the discovered problem was centered around the damage seen on the OPGaAs crystal there are two ways to fix this issue. First method being done is translating the crystal vertically in the OPO, so the main power of the beam alignment is not impacting the already damaged section of the crystal. The second option to fix this issue is to replace the OPGaAs crystal. If the OPGaAs crystal is replaced then that would also impact the second question of what is the definitive wavelength being emitted from the laser.

To resolve the question regarding the wavelength there are a couple of suggestions. First use a grating designed for the wavelength region and calculate the wavelength based on the observed first order angle of the beam through the grating. Second option would be sending the beam into a spectrometer that is also designed for this wavelength region. This would be the most realistic, however there was limited to no access to a spectrometer for this region at this time. A third suggestion to determine the wavelength would be doing fine measurements to fiber couple the light into an Optical Spectrum Analyzer to observe the emitted wavelength. As mentioned if the crystal is moved or replaced this would impact the thought of what wavelength is emitted based on the calibration of temperature and grating provided by BAE Systems.

At the time of writing the crystal has been translated and the power did increase at the calibrated temperature and grating angle. Recently repeating the Power vs Temperature method and just observing the power at 3.8 microns the results were different than shown in Table 4.1. The power measured under the same setup where the pump is blocked and the power measured is the signal and idler. As mentioned the calibrated temperature is around 165.85°C, the power was around 90 mW. Changing the temperature to 163°C, the power was observed to be over double around 200 mW. This shows the aspect of calibration being off at some point over the course of using the laser and would need adjusted as more tests and experiments using the laser are completed.

Even though the complications of the laser trumped the initial goal of find the refractive index of a variety of materials, there was still a lot learned over the course of the project. From designing and completing different testing configurations to exploring the interior components and process of the tunable MWIR laser. In terms of the laser used in this

work, only time will tell for its full potential and capabilities for experiments in the infrared spectrum.

BIBLIOGRAPHY

[1] S. Wemple, M. Didomenico, and I. Camlibel, "Dielectric and optical properties of melt-grown batio3," *Journal of Physics and Chemistry of Solids*, vol. 29, no. 10, pp. 1797–1803, 1968. [Online]. Available: https://www.sciencedirect.com/science/article/pii/0022369768901649

[2] R. J. Brecha and J. M. OHare, *Optical Radiation and Matter*, ser. 2053-2563. IOP Publishing, 2021.

[3] A. I. Lvovsky, *Fresnel Equations*. Taylor and Francis, Feb 2013, pp. 1–6.

[4] D. Tentori-Santa-Cruz and J. R. Lerma, "Refractometry by minimum deviation: accuracy analysis," *Optical Engineering*, vol. 29, no. 2, pp. 160–168, 1990. [Online]. Available: https://doi.org/10.1117/12.55573

[5] Jun 2018. [Online]. Available: https://www.jawoollam.com/resources/ellipsometry-tutorial

[6] S. A. Khan, S. B. Khan, L. U. Khan, A. Farooq, K. Akhtar, and A. M. Asiri, *Fourier Transform Infrared Spectroscopy: Fundamentals and Application in Functional Groups and Nanomaterials Characterization*. Springer International Publishing, 2018, pp. 317–344. [Online]. Available: https://doi.org/10.1007/978-3-319-92955-23em
9

[7] T. F. S. Inc., "Introduction to fourier transform infrared spectroscopy," May 2022. [Online]. Available: https://assets.thermofisher.com/TFS-Assets/MSD/brochures/introduction-fourier-transform-infrared-spectroscopy-br50555.pdf

[8] D. E. Zelmon, D. L. Small, and D. Jundt, "Infrared corrected sellmeier coefficients for congruently grown lithium niobate and 5 mol. magnesium oxide–doped lithium niobate," *J. Opt. Soc. Am. B*, vol. 14, no. 12, pp. 3319–3322, Dec 1997. [Online]. Available: https://opg.optica.org/josab/abstract.cfm?URI=josab-14-12-3319

[9] N. Umemura, K. Yoshida, and K. Kato, "Phase-matching properties of knbo3 in the mid-infrared," *Appl. Opt.*, vol. 38, no. 6, pp. 991–994, Feb 1999. [Online]. Available: https://opg.optica.org/ao/abstract.cfm?URI=ao-38-6-991

[10] B. Zysset, I. Biaggio, and P. Günter, "Refractive indices of orthorhombic knbo3. i. dispersion and temperature dependence," *J. Opt. Soc. Am. B*, vol. 9, no. 3, pp. 380–386, Mar 1992. [Online]. Available: https://opg.optica.org/josab/abstract.cfm?URI=josab-9-3-380

[11] D. T. F. Marple, "Refractive Index of ZnSe, ZnTe, and CdTe," *Journal of Applied Physics*, vol. 35, no. 3, pp. 539–542, 03 1964. [Online]. Available: https://doi.org/10.1063/1.1713411

[12] P. Xiao, X. Wang, J. Sun, M. Huang, X. Chen, and Z. Cao, "Simultaneous measurement of electro-optical and converse-piezoelectric coefficients of pmn-pt ceramics," *Opt. Express*, vol. 20, no. 13, pp. 13 833–13 840, Jun 2012. [Online]. Available: https://opg.optica.org/oe/abstract.cfm?URI=oe-20-13-13833

[13] B. S. E. Group, *Tunable Mid-IR Laser*, BAE Systems EOIR Group, Merrimack, New Hampshire.

[14] R. Paschotta, "Optical parametric oscillators," RP Photonics Encyclopedia.

[15] M. Born and E. Wolf, *Principles of Optics*. Cambridge University Press, Dec. 2019, p. 174. [Online]. Available: http://dx.doi.org/10.1017/9781108769914.004

[16] J. A. Bastin, E. W. J. Mitchell, and J. Whitehouse, "Use of an integrating sphere to distinguish between absorption and scattering in solids," *British Journal of Applied Physics*, vol. 10, no. 9, p. 412416, Sep. 1959. [Online]. Available: http://dx.doi.org/10.1088/0508-3443/10/9/308

APPENDIX A

Python Code for Analysis

A.1 Transmission at Normal Incidence

```
#Transmission at Normal Incidence Analysis
import numpy as np
import pandas as pd
import matplotlib.pyplot as plt
from scipy.optimize import fsolve
#Constants
n1 = 1
Ti = 20
#Data import
data = pd.read_table('LN_NormTran.txt', header=None, delimiter=None)
print(data)
#Experimental Results
n = np.zeros(len(data))
for i in range(len(data)):
    num = 1+np.sqrt(1-np.sqrt((data[2][i]/data[1][i])**2))
    dem = 1-np.sqrt(1-np.sqrt((data[2][i]/data[1][i])**2))
    n[i] = num/dem
#Theoretical results
noln= np.zeros(len(data))
for i in range(len(data)):
    x = data[0][i]/1000
    noln[i] = np.sqrt(1+((2.6734*x**2)/(x**2-0.01764))+((1.2290*x**2)/(x**2-
0.05914))+((12.614*x**2)/(x**2-474.6)))
#Trendline calculation
x1 = data[0]/1000
y1 = n
z = np.polyfit(x1, y1, 3)
p = np.poly1d(z)
plt.scatter(data[0]/1000, n, label="Experimental", marker='o', color='blue')
plt.plot(x1, p(x1), "b--", label="Experimental Trend")
plt.plot(data[0]/1000, noln, label="Theoretical", marker='D', color='red')
# plt.rc('figure', titlesize=20)
# plt.rc('xtick', labelsize = 12)
# plt.rc('axes', titlesize=18)
# plt.rc('ytick', labelsize = 12)
plt.title("Normal Incidence Tranmission Refractive Index")
plt.xlabel("Wavelength ($\mu$m)")
plt.ylabel("Refractive Index")
plt.legend()
plt.show()
```

A.2 Reflection Result Analysis

```
#Evaluation of Reflection Results
import numpy as np
import sympy as sp
import pandas as pd
import matplotlib.pyplot as plt
from scipy.optimize import fsolve
#Constants
n1 = 1
Ti = np.deg2rad(20)
d = 1000 #Thickness in microns to match wavelength
wl = 4.2
def Reflection1(n2):
    return ((((n1/n2)*np.cos(Ti)-np.sqrt(1-(((n1/n2)**2)*np.sin(Ti)**2)))/
                        ((n1/n2)*np.cos(Ti)+np.sqrt(1-(((n1/n2)**2)*np.sin(Ti
)**2))))**2 - R1)
def Reflection2(n2):
    return (((n1*np.cos(Ti)-n2*(np.sqrt(1-(((n1/n2)**2)*np.sin(Ti)**2))))/(
n1*np.cos(Ti)+n2*(np.sqrt(1-(((n1/n2)**2)*np.sin(Ti)**2))))**2 + (n2*(np.
sqrt(1-(((n1/n2)**2)*np.sin(Ti)**2)))-n1*np.cos(Ti))/(n1*np.cos(Ti)+n2*(np.
sqrt(1-(((n1/n2)**2)*np.sin(Ti)**2))))**2 + 2*(n1*np.cos(Ti)-n2*(np.sqrt(1-
(((n1/n2)**2)*np.sin(Ti)**2))))/(n1*np.cos(Ti)+n2*(np.sqrt(1-(((n1/n2)**2)*
np.sin(Ti)**2))))*(n2*(np.sqrt(1-(((n1/n2)**2)*np.sin(Ti)**2)))-n1*np.cos(Ti
))/(n1*np.cos(Ti)+n2*(np.sqrt(1-(((n1/n2)**2)*np.sin(Ti)**2))))*np.cos(4*np.
pi*d*(np.sqrt(1-(((n1/n2)**2)*np.sin(Ti)**2)))/wl))/(1+ ((n1*np.cos(Ti)-n2*(
np.sqrt(1-(((n1/n2)**2)*np.sin(Ti)**2))))/(n1*np.cos(Ti)+n2*(np.sqrt(1-(((n1
/n2)**2)*np.sin(Ti)**2))))*(n2*(np.sqrt(1-(((n1/n2)**2)*np.sin(Ti)**2)))-n1*
np.cos(Ti))/(n1*np.cos(Ti)+n2*(np.sqrt(1-(((n1/n2)**2)*np.sin(Ti)**2)))))**2
 + 2*(n1*np.cos(Ti)-n2*(np.sqrt(1-(((n1/n2)**2)*np.sin(Ti)**2))))/(n1*np.cos
(Ti)+n2*(np.sqrt(1-(((n1/n2)**2)*np.sin(Ti)**2))))*(n2*(np.sqrt(1-(((n1/n2)
**2)*np.sin(Ti)**2)))-n1*np.cos(Ti))/(n1*np.cos(Ti)+n2*(np.sqrt(1-(((n1/n2)
**2)*np.sin(Ti)**2))))*np.cos(4*np.pi*d*(np.sqrt(1-(((n1/n2)**2)*np.sin(Ti)
**2)))/wl))-R2)
#Import of Data
LN1 = pd.read_table("May1Test.txt", header=None, delimiter=None)
LN2 = pd.read_table("May13Test.txt", header=None, delimiter=None)
#Bypass the For Loop and Solve for a single point
R1 = 1.820/8.678
R2 = 1.132/4.478
nssr = fsolve(Reflection1, 2.0)
ndsr = fsolve(Reflection2, 2.0)
print(nssr, ndsr)
#Theoretical results
noln= np.zeros(len(LN2))
for i in range(len(LN2)):
    x = LN2[0][i]/1000
    noln[i] = np.sqrt(1+((2.6734*x**2)/(x**2-0.01764))+((1.2290*x**2)/(x**2-
0.05914))+((12.614*x**2)/(x**2-474.6)))
ndsr2 = np.zeros(len(LN2))
for i in range(len(LN2)):
    wl = LN2[0][i]
    #R2 = LN1[2][i]/(LN1[1][i]/LN1[4][0])
    R2 = LN2[3][i]/LN2[1][i]
    ndsr2[i]=fsolve(Reflection2, 2.0)
print(ndsr2)
plt.scatter(LN1[0], ndsr2, color='blue', label='Experimental')
plt.plot(LN1[0], noln, 'g--', label='Expected')
plt.title('LiNbO$_3$ Reflection Tests Refractive Index')
plt.xlabel("Wavelength (nm)")
plt.ylabel("Refractive Index")
plt.legend()
plt.show()
```

A.3 Transmission at Angle of Incidence

```
#Evaluation of Transmission data results
import numpy as np
import pandas as pd
import matplotlib.pyplot as plt
from scipy.optimize import fsolve
#Constants
n1 = 1
Ti = 20
#Define equation for solving
def T_hor(n2):
    Tt = np.sqrt(1-(((n1/n2)**2)*np.sin(Ti)*np.sin(Ti)))
    return (4*(n1/n2)*np.cos(Ti)-Tt)/(((n1/n2)*np.cos(Ti)+Tt)**2) - Thor
#Import of Data
LN1 = pd.read_table("May1Test.txt", header=None, delimiter=None)
LN2 = pd.read_table("May13Test.txt", header=None, delimiter=None)
Tnln1 = np.zeros(len(LN1))
for i in range(len(LN1)):
    bs = LN1[4][i]
    Thor = np.sqrt(LN1[3][i]/(LN1[1][i]/bs))   #Obtaining Reflectance from
                                               data
    Tnln1[i] = fsolve(T_hor, 1.0)             #Fsolve for Refractive Index and
                                               store in array
print(Tnln1)
Tnln2 = np.zeros(len(LN2))
for i in range(len(LN2)):
    Thor = np.sqrt(LN2[4][i]/(LN2[1][i]))    #Obtaining Reflectance from data
    Tnln2[i] = fsolve(T_hor, 1.0)             #Fsolve for Refractive Index and
                                               store in array
print(Tnln2)
#Theoretical results
noln= np.zeros(len(LN1))
for i in range(len(LN1)):
    x = LN1[0][i]/1000
    noln[i] = np.sqrt(1+((2.6734*x**2)/(x**2-0.01764))+((1.2290*x**2)/(x**2-
0.05914))+((12.614*x**2)/(x**2-474.6)))
#Plot of the data results
plt.scatter(LN1[0], Tnln1, color='blue', label='Test 1 data')
plt.scatter(LN2[0], Tnln2, color='red', label='Test 2 data')
plt.plot(LN1[0], noln, color='green', label='Expected')
plt.title('LiNb0$_3$ Transmission Tests Refractive Index')
plt.xlabel("Wavelength (nm)")
plt.ylabel("Refractive Index")
plt.legend()
plt.show()
```

A.4 Single Wavlength Transmission Analysis

```
#Transmission Data analysis via system of equations
'''Transmission Measurement Tests
This code file will utilize one equation with varied angle of incidence.
By making the only change the incidence angle this method is simple
solving a system of equations (2 Equations; 2 unknowns).
The values solved in the system of equations is the refractive index, n,
and the absorption, alpha, which contributes to the imaginary component, k.
'''
import numpy as np
import sympy as sp
import mpmath
import pandas as pd
from scipy import optimize
import matplotlib.pyplot as plt
#Equation at normal incidence
# T = (1-R)**2 * exp(-alpha*d) / 1 - R**2 * exp(-2alpha*d)
# R = 1-n2/1+n2
#Equation at some angle of incidence
# T = (1-R)**2 * exp(-alpha*d/cos(theta2)) / 1 - R**2*exp(-alpha*d/cos(
                                        theta2))
# R = cos(theta1) - n2*cos(theta2)/ cos(theta1)+n2*cos(theta2)
# cos(theta2) = sqrt(n2**2 - n1**2*sin**2(theta1))
#Import of Data
# Angle of Incidence (deg), Inc. Power, Trans. Power
Data = pd.read_table("NewData.txt", header=None, delimiter=None)
Data2 = pd.read_table("NewData2.txt", header=None, delimiter=None)
#Symbols
n2 = sp.Symbol('n2')
a = sp.Symbol('a')
#Constants
d = 0.1      #Thickness of Material in cm
# Angle of Incidence
Ti = np.deg2rad(20)
# T Calculation: T = Trans. Power / Inc. Power
T1 = np.zeros(len(Data))
for i in range(len(Data)):
    T1[i] = Data[2][i]/Data[1][i]
T1norm = T1[0]
T1angle = T1[4]
T2 = np.zeros(len(Data2))
for i in range(len(Data2)):
    T2[i] = Data2[2][i]/Data2[1][i]
print(T1)
print(T2)
#Same Dataset but use scipy/fsolve to determine the unknowns
#Define equations
def func(n):
    return [((1-((n[0]-1)/(n[0]+1))**2)**2*np.exp(-n[1]*d)/(1-(((n[0]-1)/(n[
0]+1))**2)**2*np.exp(-2*n[1]*d)))-T1[0],
            ((1-((np.cos(Ti)-(n[0]*np.sqrt(n[0]**2-np.sin(Ti)**2)))/(np.cos(
Ti)+(n[0]*np.sqrt(n[0]**2-np.sin(Ti)**2))))**2)**2*np.exp(-n[1]*d/np.sqrt(n[
0]**2-np.sin(Ti)**2)))/(1-((((np.cos(Ti)-(n[0]*np.sqrt(n[0]**2-np.sin(Ti)**2
)))/(np.cos(Ti)+(n[0]*np.sqrt(n[0]**2-np.sin(Ti)**2))))**2)**2)*np.exp(-2*n[
1]*d/np.sqrt(n[0]**2-np.sin(Ti)**2)))-T1[4]]
def func20(n):
    return [((1-((n[0]-1)/(n[0]+1))**2)**2*np.exp(-n[1]*d)/(1-(((n[0]-1)/(n[
0]+1))**2)**2*np.exp(-2*n[1]*d)))-T2[0],
            ((1-((np.cos(Ti)-(n[0]*np.sqrt(n[0]**2-np.sin(Ti)**2)))/(np.cos(
Ti)+(n[0]*np.sqrt(n[0]**2-np.sin(Ti)**2))))**2)**2*np.exp(-n[1]*d/np.sqrt(n[
0]**2-np.sin(Ti)**2)))/(1-((((np.cos(Ti)-(n[0]*np.sqrt(n[0]**2-np.sin(Ti)**2
)))/(np.cos(Ti)+(n[0]*np.sqrt(n[0]**2-np.sin(Ti)**2))))**2)**2)*np.exp(-2*n[
1]*d/np.sqrt(n[0]**2-np.sin(Ti)**2)))-T2[2]]
def func10(n):
    return [((1-((n[0]-1)/(n[0]+1))**2)**2*np.exp(-n[1]*d)/(1-(((n[0]-1)/(n[
0]+1))**2)**2*np.exp(-2*n[1]*d)))-T2[0],
            ((1-((np.cos(Ti)-(n[0]*np.sqrt(n[0]**2-np.sin(Ti)**2)))/(np.cos(
Ti)+(n[0]*np.sqrt(n[0]**2-np.sin(Ti)**2))))**2)**2*np.exp(-n[1]*d/np.sqrt(n[
0]**2-np.sin(Ti)**2)))/(1-((((np.cos(Ti)-(n[0]*np.sqrt(n[0]**2-np.sin(Ti)**2
)))/(np.cos(Ti)+(n[0]*np.sqrt(n[0]**2-np.sin(Ti)**2))))**2)**2)*np.exp(-2*n[
1]*d/np.sqrt(n[0]**2-np.sin(Ti)**2)))-T2[1]]
Results2_1 = optimize.fsolve(func,[2, 0.01])
Results2_2 = optimize.fsolve(func20,[2, 0.01])
```

```
print(Results2_1)
print(Results2_2)
""" Results3 = fsolve(func20,[1,1])
print(Results3)
Results4 = fsolve(func10, [1,1])
print(Results4) """
#Look at the value of refractive index assuming the transmission value and
                                        assuming 0.1 as the absoption term
print("Compare")
```